Fibers and Polymers 2020, Vol.21, No.3, 473-479
DOI 10.1007/s12221-020-9803-1

ISSN 1229-9197 (print version)
ISSN 1875-0052 (electronic version)

Fabrication and Characterization of Piezoelectric Composite Nanofibers Based on Poly(vinylidene fluoride-*co*-hexafluoropropylene) and Barium Titanate Nanoparticle

Sang Hoon Lee, Young Chul Choi, Min Su Kim, Kyung Moon Ryu, and Young Gyu Jeong*

Department of Advanced Organic Materials and Textile System Engineering, Chungnam National University, Daejeon 34134, Korea

(Received July 25, 2019; Revised August 25, 2019; Accepted August 27, 2019)

Abstract: Poly(vinylidene fluoride-*co*-hexafluoropropylene) (PVDF-HFP)-based composite nanofibers containing different barium titanate ($BaTiO_3$) nanoparticle contents of 10-60 wt% were fabricated by an efficient electrospinning. The piezoelectric performance of PVDF-HFP/$BaTiO_3$ composite nanofibers under a periodic compressional pressure of ~20 kPa was investigated by considering the $BaTiO_3$ content and the electric poling. The X-ray diffraction patterns revealed the presence of piezoelectric tetragonal $BaTiO_3$ nanoparticles in the composite nanofibers with PVDF β-form crystals. The SEM images demonstrated that the $BaTiO_3$ nanoparticles were dispersed uniformly in the composite nanofibers at relatively low loadings of 10-20 wt%, but they formed aggregates at high loadings of 30-60 wt%. The piezoelectric performance of the composite nanofibers increased with the $BaTiO_3$ content up to 20 wt% and decreased at higher $BaTiO_3$ contents of 30-60 wt%, which results from the trade-off effect between the piezoelectric performance and the dispersibility of $BaTiO_3$ nanoparticles in the composite nanofibers. Accordingly, the composite nanofibers with 20 wt% $BaTiO_3$ exhibited maximum piezoelectric outputs such as voltage of ~9.63 V, current ~0.52 μA, and electric power of ~7892.2 nW. After the electric poling, the piezoelectric performance was further enhanced to ~11.69 V, ~20.56 μA, and ~1115.2 nW, which was high enough to light up a small LED bulb after rectification.

Keywords: PVDF-HFP, Electrospinning, Composite nanofibers, $BaTiO_3$ nanoparticle, Piezoelectricity

Introduction

The piezoelectric effect converts mechanical energy in the form of vibrations or shocks into electrical energy [1,2]. Piezoelectric energy harvesters offer a robust and reliable solution by converting normally wasted vibrational energy in the environment to usable electrical energy. Therefore, they can be ideal in applications that need to charge energy storage devices including battery and supercapacitor, or to power directly remote sensor systems and wearable devices for personal health care and environmental monitoring [3-7].

Energy harvesting techniques based on the piezoelectric effect have been realized by the fabrication of a variety of crystalline inorganic ceramics and polymers. In cases of wearable devices and sensors, flexible piezoelectric materials need to be developed by introducing piezoelectric inorganic materials such as lead zirconate titanate (PZT), zinc oxide (ZnO), and barium titanate ($BaTiO_3$) to flexible polymeric materials [8-10]. As a piezoelectric inorganic material, PZT is known to have toxic heavy metals such as lead (Pb) more than 60 wt%, which leads to causing environmental pollution in production or harmful effects to human body [11]. Accordingly, $BaTiO_3$ in a variety of shapes of nanotubes [12], nanoparticles [13,14], nanowires [15], and nanofibers [9,16] has been investigated as a non-lead inorganic material with high piezoelectric coefficient and dielectric constant [17-19].

*Corresponding author: ygjeong@cnu.ac.kr

Poly(vinylidene fluoride) (PVDF) and its copolymers have been widely investigated as piezoelectric polymeric materials with excellent thermal, dielectric, and mechanical properties [20-22]. It has been reported that PVDF has various crystal phases of α-, β-, γ-, δ- and ε-forms, and its mechanical and dielectric properties vary depending on the crystal phases [23,24]. Accordingly, the crystal phase control of PVDF is one of critical factors for attaining high piezoelectricity [25,26]. PVDF chain backbones take all trans conformations in the β-form, TGTG' (trans-gauche-trans-gauche) conformations in the α- and δ-forms, and T_3GT_3G' conformations in the γ- and ε-forms [23]. Among those crystal phases, the α- and ε-forms do not have piezoelectric properties, because the dipoles are packed antiparallel within the unit cells. On the other hand, the β- and γ-forms have piezoelectric properties, because the F and H atoms are biased to one side, thereby forming a spontaneous polarization in the overall polymer chains. In particular, the β-form is known to have the highest piezoelectric property because it has a higher dipolar moment per unit cell, compared to the γ-form. It is thus critical to develop the β-form crystals to obtain high piezoelectricity. For producing typical commercial piezoelectric PVDF thin films, relatively high electrical potential and mechanical stretching are necessary at elevated temperatures [27]. On the other hand, electrospinning is an effective process to fabricate nanofibers under a high bias voltage above 10 kV, which can transform non-polar crystal phases to polar crystal phases with improved piezoelectricity [28-30].

On continuing the efforts to attain flexible and high performance piezoelectric materials, in this study, we fabricated a series of composite nanofibers based on poly(vinylidene fluoride-*co*-hexafluoropropylene) (PVDF-HFP) and $BaTiO_3$ nanoparticles by adopting an efficient electrospinning technique. The morphological and microstructural features of PVDF-HFP/$BaTiO_3$ composite nanofibers were characterized by using SEM, Raman, FT-IR, and X-ray diffraction methods. The time-dependent piezoelectric voltage and current changes of the composite nanofibers under a constant periodic compressional stress of ~20 kPa were monitored by using a multimeter. The microstructure and piezoelectric performance of PVDF-HFP/$BaTiO_3$ composite nanofibers were investigated systematically by taking into account the $BaTiO_3$ content (0-60 wt%) and electric poling effect.

Experimental

Materials

PVDF-HFP (400,000 g/mol, Sigma-Aldrich Com.) was used as a piezoelectric PVDF-based copolymer for fabricating electrospun composite nanofibers. Barium titanate ($BaTiO_3$, Sigma-Aldrich Com.) with the cubic phase and the particle size of <50 nm was sintered at 1000 °C for 2 hr to obtain piezoelectric tetragonal nanocrystals. N,N-dimethylformaide (DMF, Samchun Pure Chemical Co., 99.0 %) and acetone (Samchun Pure Chemical Co., 99.5 %) were used as solvents for preparing electrospinning dopes containing PVDF-HFP and $BaTiO_3$ nanocrystals. Polydimethylsiloxane (PDMS, SYLGARD 184 silicone elastomer kit, Dow Corning Cor.) was used as an elastomeric binder for composite nanofiber webs.

Fabrication of PVDF-HFP/$BaTiO_3$ Composite Nanofibers as Piezoelectric Generators

The PVDF-HFP-based composite nanofibers containing different $BaTiO_3$ contents of 10-60 wt% were fabricated by an electrospinning. First, 0.65 g PVDF-HFP was dissolved in a mixed solvent of 21 m*l* DMF and 9 m*l* acetone in an encapsulated container, which was then heated at 60 °C for 1 hr and cooled to ambient temperature for 0.5 hr. Second, predetermined amount of $BaTiO_3$ nanoparticles (10-60 wt% of PVDF-HFP) was added in the solution and stirred for 2 hr. Third, PVDF-HFP/$BaTiO_3$/DMF/acetone solution in a syringe with an inner diameter of 21G was electrospun to a rotating collector at a feed rate of 0.5 m*l*/hr, electric field of 13-15 kV, and distance between the syringe tip and the collector of 25 cm. Finally, the electrospun PVDF-HFP/$BaTiO_3$ composite nanofiber webs were dried at room temperature for overnight. For comparison, neat PVDF-HFP nanofiber webs were also fabricated at the same procedure.

The piezoelectric energy generators based on PVDF-HFP/$BaTiO_3$ composite nanofibers were fabricated as follows. First, PDMS binder dissolved in chloroform was applied to neat PVDF-HFP and PVDF-HFP/$BaTiO_3$ composite nanofiber webs with 2.5 cm×2.5 cm and then dried at 60 °C for 5 min to remove chloroform solvent. Second, the nanofiber webs with PDMS binder were placed between two Cu-coated polyimide films as electrodes and then cured in an oven at 80 °C for 2 hr. Finally, PVDF-HFP/$BaTiO_3$ composite nanofibers with top and bottom electrodes were kept in ambient condition for 24 hr.

To investigate the influence of electric poling on the piezoelectric performance of PVDF-HFP/$BaTiO_3$ composite nanofibers, the electric field of 25 kV/cm was applied to the composite nanofiber webs between two electrodes in silicone oil bath at 80 °C. After the poling process, the composite nanofiber webs between two electrodes were washed with methanol to remove the silicone oil and dried at room temperature for 24 hr.

Characterization

The morphological features of neat PVDF-HFP nanofibers and PVDF-HFP/$BaTiO_3$ composite nanofibers were characterized by using a cold type field emission scanning electron microscope (ZEISS, Merlin compact). The crystal structure changes of $BaTiO_3$ nanoparticles before and after the sintering process were identified by using Raman spectroscopy (HORIBA JOBIN YVON, LabRAM HR-800). The crystalline structures of the neat and composite nanofibers were determined by a high performance X-ray diffractometer using Cu-Kα radiation (D8 DISCOVER, Bruker AXS) and FT-IR spectrometer (iS10, Thermo). Time-dependent piezoelectric voltage and current generations of the neat and composite nanofibers under a periodic compressional pressure of ~20 kPa were monitored with aid of 7½-digit graphical sampling multimeter (DMM7510, Keithley). For the experiment, the periodic compressional pressure was applied manually to the composite nanofiber webs between Cu-coated polyimide film electrodes by using finger tap with ~2 N force and ~1 cm^2 area. The alternating voltage outputs generated by the periodic compressional pressure were rectified to light up a small light emitting diode (LED) bulb to confirm practical applicability of PVDF-HFP/$BaTiO_3$ composite nanofibers as piezoelectric energy harvesters.

Results and Discussion

Morphological and Structural Characterization

Figure 1 shows SEM images of the neat PVDF-HFP and its composite nanofibers containing different $BaTiO_3$ contents of 10-60 wt%. The SEM images revealed that all the nanofibers were formed uniformly in shape during the electrospinning process, although aggregates of $BaTiO_3$ nanoparticles increased in the composite nanofibers with relatively high $BaTiO_3$ contents of 30-60 wt%. For the neat PVDF-HFP nanofibers, the average diameter was measured

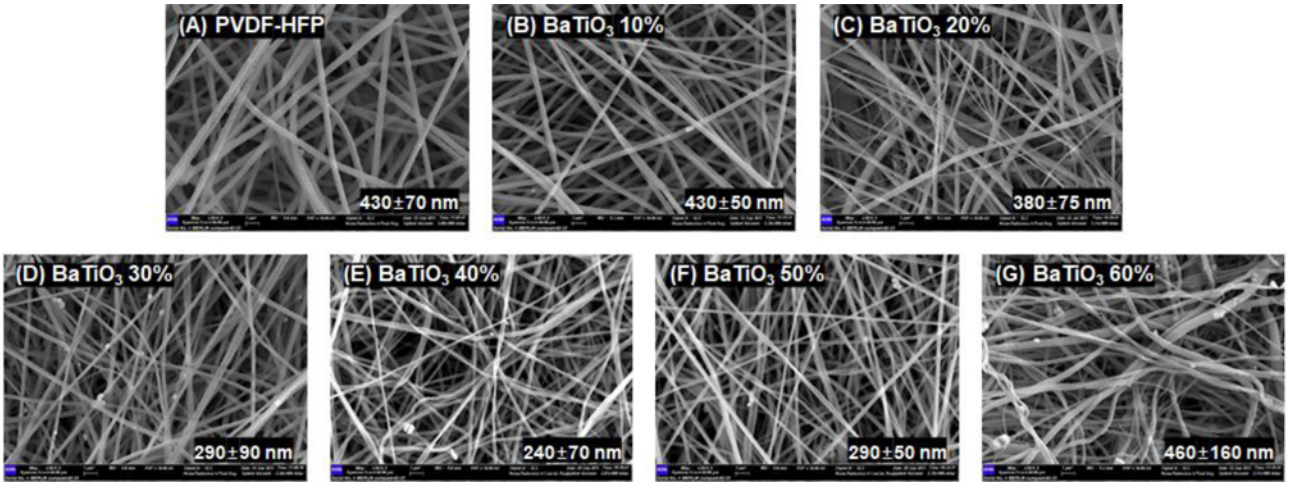

Figure 1. SEM images of neat PVDF-HFP nanofiber (A) and composite nanofibers (B-G) with different $BaTiO_3$ content of 10-60 wt%.

to be ~430 nm. In cases of the composite fibers, the average diameters decreased to ~240 nm with increasing the $BaTiO_3$ content up to 40 wt%, but they increased again to ~460 nm at higher $BaTiO_3$ loading of 60 wt%. The changes of the average diameter of the composite nanofibers with the $BaTiO_3$ content is believed to be associated with the combinatorial effect of good electric/dielectric property and poor dispersibility of $BaTiO_3$ nanoparticles. The $BaTiO_3$ nanoparticles with relatively high dielectric constant contribute to form nanofibers with smaller diameters, while the high amounts of $BaTiO_3$ induced the formation of thicker nanofibers with $BaTiO_3$ aggregates owing to the poor dispersion. On the other hand, The aggregates of $BaTiO_3$ nanoparticles can act as defects by deteriorating the mechanical and piezoelectric properties of the nanofibers [31].

The crystal structure of $BaTiO_3$ is known to be an important factor for obtaining a high piezoelectric constant [32]. The tetragonal crystal structure of $BaTiO_3$ exhibits ferroelectricity that has a spontaneous polarization due to the biased electric property induced by the twisted crystal lattice, whereas the cubic crystal structure does not have spontaneous polarization and thus has no piezoelectricity [33,34]. The crystal structure of $BaTiO_3$ nanoparticle can be confirmed by X-ray diffraction and Raman spectroscopy [35,36]. However, since the difference between X-ray diffraction patterns of the cubic and tetragonal phases is very small, Raman spectroscopic analysis is rather advantageous to confirm the crystal structure of $BaTiO_3$ [36]. In general, it has been known that, unlike the cubic phase (*Pm3m*), the tetragonal phase (*P4mm*) $BaTiO_3$ nanoparticles have Raman-active modes of $4E$(TO+LO), $3A_1$(TO+LO) and B_1(TO+LO) due to non-centrosymmetric properties [37,38]. To identify the crystal structure of $BaTiO_3$ nanoparticles, the Raman spectra of $BaTiO_3$ nanoparticles before and after the sintering process were obtained, as represented in Figure 2.

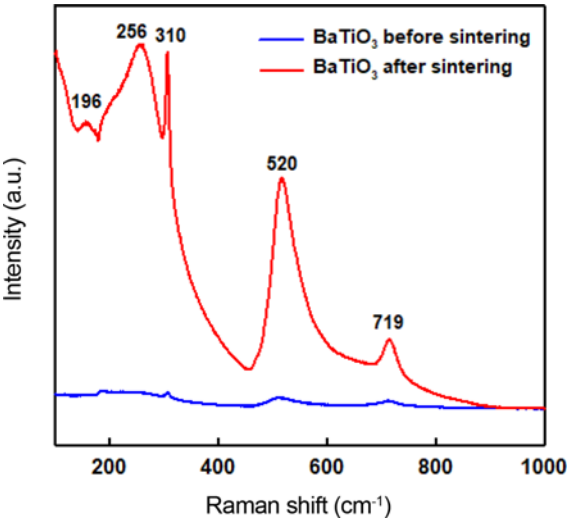

Figure 2. Raman spectra of $BaTiO_3$ nanoparticles before and after sintering at 1000 °C for 2 hr.

As a result, it was found that $BaTiO_3$ nanoparticles after the sintering process exhibited typical Raman-active modes of the tetragonal phase at 196, 256, 310, 520, and 720 cm^{-1}, which are assigned to A_1(TO)/E(LO), A_1(TO), B_1(TO+LO)/E, A_1(TO)/E, and A_1(LO)/E, respectively [39-41]. It is thus valid to contend that $BaTiO_3$ nanoparticles obtained by the sintering process are in the piezoelectric tetragonal crystal phase.

To characterize the crystalline phase of PVDF-HFP component in the composite nanofibers, FT-IR spectra of neat PVDF-HFP and its composite nanofibers with different $BaTiO_3$ contents were obtained, as shown in Figure 3. All FT-IR spectra were found to be identical, irrespective of the $BaTiO_3$ content, by showing the characteristic bands of PVDF-HFP at 840, 880, 1172, 1279, and 1401 cm^{-1}, which originate from the vibrational modes of CH_2 bending and

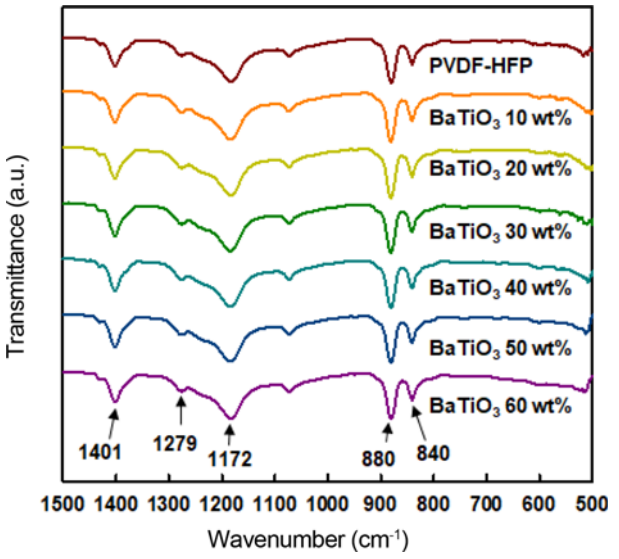

Figure 3. FT-IR spectra of neat PVDF-HFP nanofiber and composite nanofibers with different $BaTiO_3$ contents of 10-60 wt%.

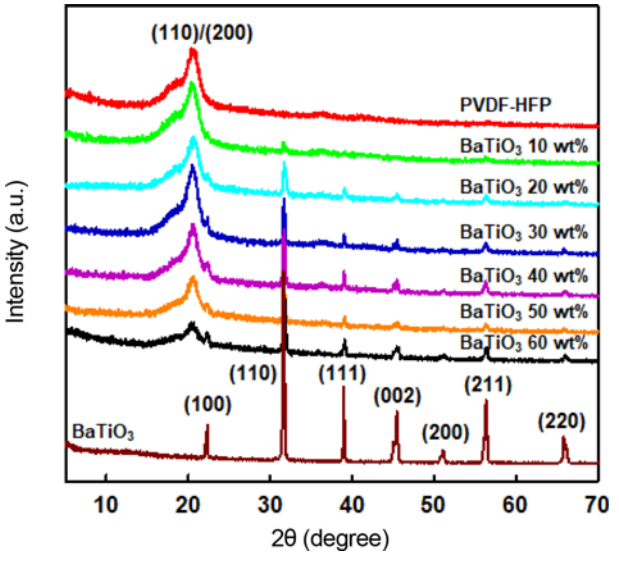

Figure 4. X-ray diffraction patterns of neat PVDF-HFP nanofiber, $BaTiO_3$ nanoparticle, and composite nanofibers with different $BaTiO_3$ contents of 10-60 wt%.

CF_2 stretching. Especially, the bands at 880 and 1279 cm^{-1} are associated with the CF_2 stretching and CH_2 wagging in the β-phase PVDF crystals, respectively [23]. On the other hand, the α-phase PVDF crystals were known to show typical vibrational bands at 489, 614, 766, 795, 855 and 976 cm^{-1} [42], which were not detected in FT-IR spectra of Figure 3. It is thus concluded that the piezoelectric β-phase PVDF crystals were developed successfully in the neat and composite nanofibers during the electrospinning process and the $BaTiO_3$ content does not influence the crystalline structure of PVDF-HFP component in the nanofibers.

Figure 4 shows the X-ray diffraction patterns of neat PVDF-HFP nanofibers and PVDF-HFP/$BaTiO_3$ composite nanofibers. For the neat PVDF-HFP nanofibers, a strong diffraction peak was detected at 20.26 °, which corresponds to (110)/(220) reflections of the β-phase PVDF crystal [43]. On the other hand, sharp and strong diffraction peaks of $BaTiO_3$ nanoparticles was detected at 22, 31, 39, 45, 51, 56, and 66 °, which stem from (100), (110), (111), (002), (200), (211), and (220) reflections of the tetragonal phase, respectively [44]. In cases of PVDF-HFP/$BaTiO_3$ composite nanofibers, all the characteristic diffraction peaks associated with the β-phase PVDF crystal and the tetragonal $BaTiO_3$ crystal were detected, although the diffraction intensities were dependent on the relative composition of PVDF-HFP and $BaTiO_3$ in the composite nanofibers. From above Raman, FT-IR and X-ray diffraction analyses, it is reasonable to contend that piezoelectric tetragonal $BaTiO_3$ nanoparticles were successfully introduced to the composite nanofibers based on PVDF-HFP matrix with β-phase PVDF crystals.

Piezoelectric Performance of PVDF-HFP/$BaTiO_3$ Composite Nanofibers

The piezoelectric properties of the neat PVDF-HFP and its composite nanofibers with different $BaTiO_3$ contents were characterized by applying a periodic compressional pressure of ~20 kPa. Figure 5 shows the time-dependent output voltage and current changes under the periodic compressional pressure. When the mechanical pressure was applied to the composite nanofibers, the piezoelectric potential generated by $BaTiO_3$ nanoparticles as well as PVDF crystals leads charges to flow through an external circuit connected to top and bottom electrodes, which leads to a positive peak. Subsequently, when the applied pressure was released, the charges flow back to the opposite direction, which results in a negative peak [10,16]. On the other hand, by using the time-dependent output voltage data of Figure 5(A), the output electric powers of the composite nanofibers could be calculated according to the following equation [10,45]:

$$P = \frac{1}{T}\int \frac{U^2(t)}{R} dt \quad (1)$$

where $U^2(t)$ is the square of the real-time voltage external load, R is the impedance of the external load (10 MΩ), T is the period of pressing and releasing. By using the equation (1), the output electric powers of neat PVDF-HFP nanofibers and PVDF-HFP/$BaTiO_3$ composite nanofibers could be calculated. For comparison, the overall piezoelectric voltage, current and electric power outputs of neat PVDF-HFP and its composite nanofibers were represented as a function of the $BaTiO_3$ content, as shown in Figure 6. For the neat PVDF-HFP nanofibers, very low piezoelectric outputs such as voltage of 0.15±0.06 V, current of 0.01±

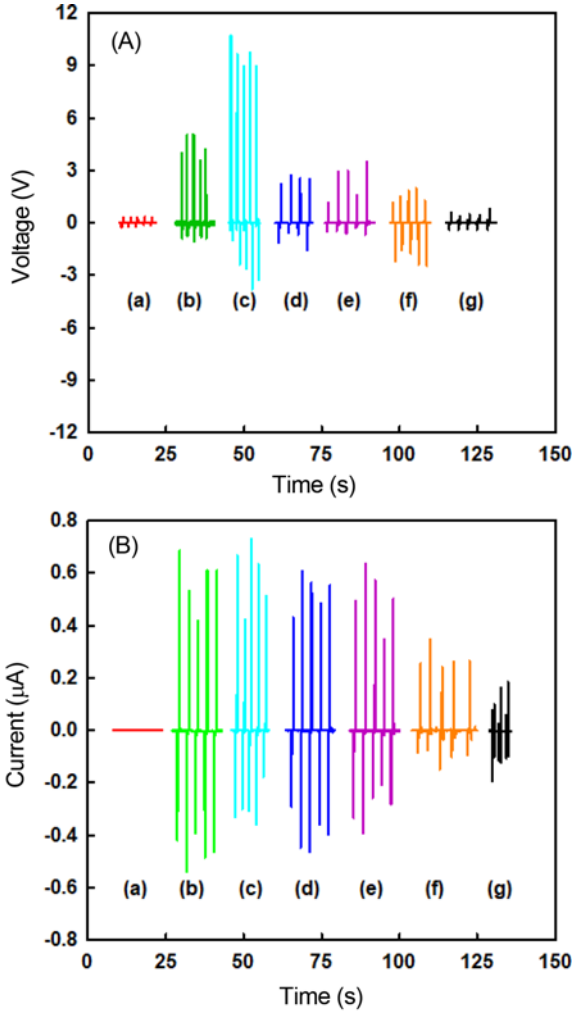

Figure 5. Time-dependent piezoelectric (A) voltage and (B) current changes under a periodic compressional stress of ~20 kPa of composite nanofibers with different $BaTiO_3$ contents; (a) neat PVDF-HFP, (b) 10 wt% $BaTiO_3$, (c) 20 wt% $BaTiO_3$, (d) 30 wt% $BaTiO_3$, (e) 40 wt% $BaTiO_3$, (f) 50 wt% $BaTiO_3$, and (f) 60 wt% $BaTiO_3$.

0.01 μA, and electric power of 1.44±0.02 nW were generated. In cases of the composite nanofibers, the piezoelectric voltage, current, and electric power outputs increased significantly with increasing the $BaTiO_3$ content up to 20 wt%, but they decreased noticeably at higher $BaTiO_3$ contents of 30-60 wt%. As the result, PVDF-HFP composite nanofiber with 20 wt% $BaTiO_3$ exhibited the highest piezoelectric outputs of 9.63±0.71 V, 0.48±0.10 μA, and 792.2±27.6 nW. The existence of maximum piezoelectric performance for the composites as a function of $BaTiO_3$ content was also reported in other literatures [10,12]. In general, it is conjectured that the piezoelectric performance of PVDF-HFP/$BaTiO_3$ composite nanofibers should be increased with the $BaTiO_3$ content. On the other hand, the

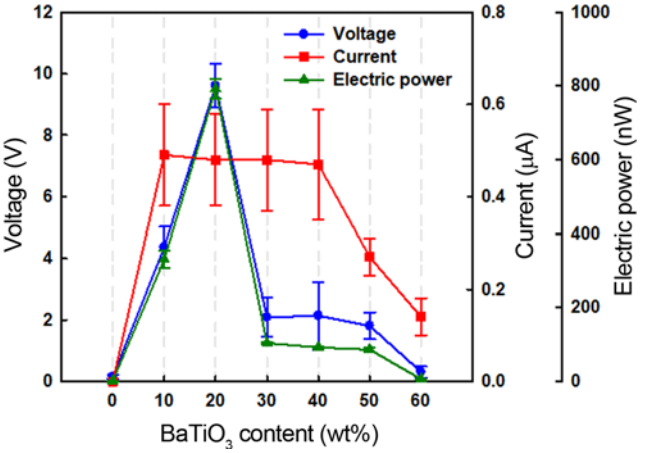

Figure 6. Piezoelectric voltage, current, and electric power outputs of PVDF-HFP/$BaTiO_3$ composite nanofibers as a function of the $BaTiO_3$ content.

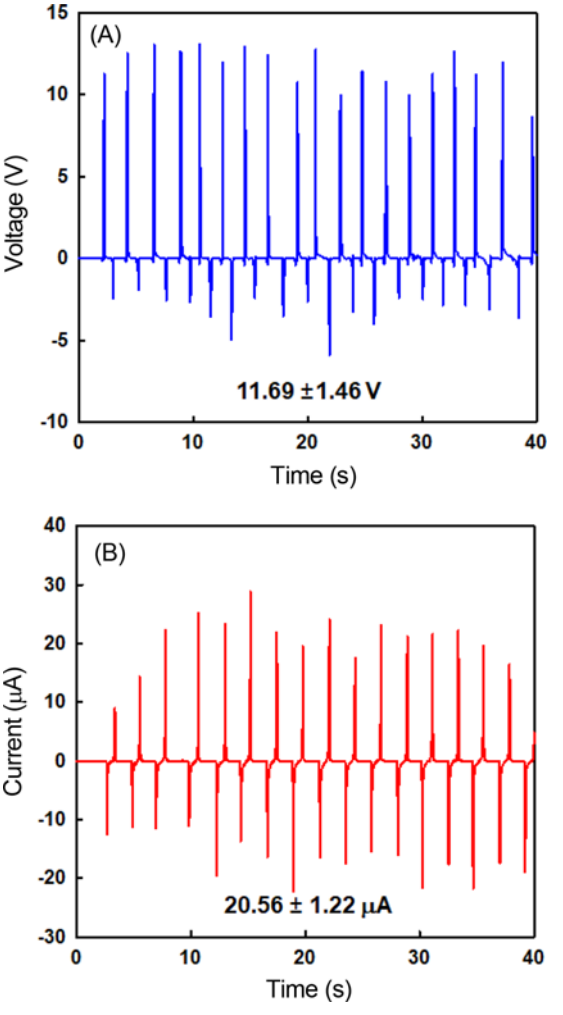

Figure 7. Time-dependent piezoelectric (A) voltage and (B) current changes of electrically poled composite nanofiber with 20 wt% $BaTiO_3$.

deteriorated piezoelectric performance for the composite nanofibers with high $BaTiO_3$ contents of 30-60 wt% is believed to be caused by the decreased dispersion of $BaTiO_3$ nanoparticles in the composite nanofibers, as supported by the SEM images. It is thus believed that the optimum $BaTiO_3$ content on the piezoelectric performance of the composite nanofibers under a constant compressional pressure is determined by the combinational effect of the piezoelectric coefficient (d_{33}~191 pC/N) and the dispersion of $BaTiO_3$ nanoparticles.

The electric poling effect on the piezoelectric performance of PVDF-HFP/$BaTiO_3$ composite nanofibers was also investigated. For the purpose, the composite nanofiber with 20 wt% $BaTiO_3$ loading was electrically poled and its time-dependent voltage and current outputs under the periodic mechanical compression were obtained, as can be seen in Figure 7. As a result, the electrically poled PVDF-HFP/$BaTiO_3$ composite nanofibers attained highly improved piezoelectric outputs such as voltage of ~11.69 V, current of ~20.56 μA, and electric power of ~1115.2 nW, which were far higher than those (~9.63 V, ~0.52 μA, and ~792.2 nW) of the unpoled counterpart. This substantial increment in the piezoelectric outputs is caused by the fact that the polarization directions of both PVDF β-crystals and tetragonal $BaTiO_3$ nanoparticles could be aligned to the perpendicular directions of the composite nanofiber webs during the electric poling process [16].

To confirm the practical applicability of PVDF-HFP/$BaTiO_3$ composite nanofibers as piezoelectric energy harvesters, the electrically poled composite nanofibers with 20 wt% $BaTiO_3$ was connected to a commercial light-emitting diode (LED) through a bridge rectifier consisting of four diodes, which converts the generated AC to DC signals, as can be seen in Figure 8. As a result, it was found that a small LED bulb, which operates at above 2 V, was lit up by the piezoelectric outputs harvested by the relatively low compressional pressure applied to PVDF-HFP/$BaTiO_3$ composite nanofibers.

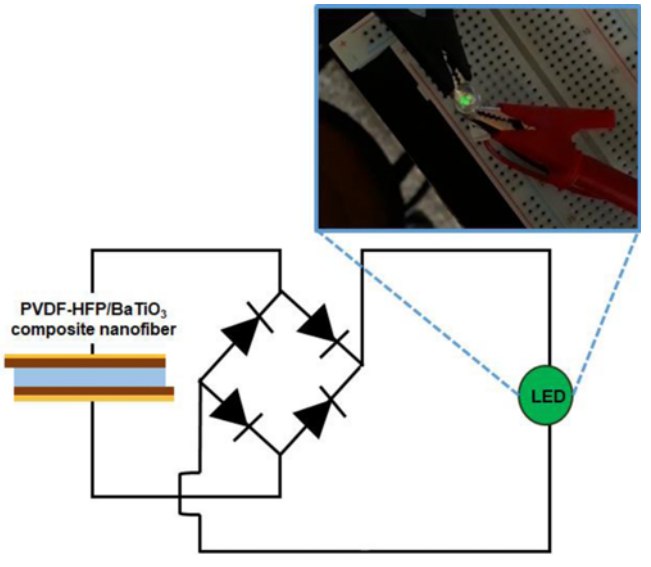

Figure 8. Schematic circuit diagram of a bridge rectifier consisting four diodes, which connects the electrically poled composite nanofiber with 20 wt% $BaTiO_3$ to a small light-emitting diode (LED) bulb.

Conclusion

In summary, PVDF-HFP-based composite nanofibers containing different contents (10-60 wt%) of $BaTiO_3$ nanoparticles in tetragonal phase were fabricated via the facile electrospinning process. The influence of the $BaTiO_3$ content and electric poling on the piezoelectric performance of PVDF-HFP/$BaTiO_3$ composite nanofibers was investigated. The FT-IR spectra and X-ray diffraction patterns revealed that the β-phase PVDF crystals was successfully developed in the composite nanofibers and the tetragonal phase of $BaTiO_3$ remained unchanged. The piezoelectric voltage, current, and electric power outputs harvested by PVDF-HFP/$BaTiO_3$ composite nanofibers were far higher than those of neat PVDF-HFP nanofibers and they were dependent on the content of $BaTiO_3$ in the composite nanofibers. The composite nanofibers with 20 wt% $BaTiO_3$ could harvest a maximum piezoelectric voltage of ~9.63 V, current of ~0.52 μA, and electric power of ~792.2 nW under an applied compression stress of ~20 kPa. When the composite nanofibers with 20 wt% $BaTiO_3$ was electrically poled, far higher piezoelectric outputs of ~11.69 V, ~20.56 μA, and ~1115.2 nW were attained, which was found to be high enough to light up a small LED bulb. Overall, it is reasonable to contend that PVDF-HFP/$BaTiO_3$ composite nanofibers with flexible and high performance piezoelectric outputs can be utilized in powering self-sufficient wearable devices, sensors, and wireless electronics.

Acknowledgements

This work was supported by the National Research Foundation of Korea (NRF) Grant funded by the Korea government (No. 2016R1D1A1B03932942).

References

1. J. Chang, M. Dommer, C. Chang, and L. Lin, *Nano Energy*, **1**, 356 (2012).
2. S. Siddiqui, D.-I. Kim, M. T. Nguyen, S. Muhammad, W.-S. Yoon, and N.-E. Lee, *Nano Energy*, **15**, 177 (2015).
3. M. A. Hannan, S. Mutashar, S. A. Samad, and A. Hussain, *BioMed. Eng. Online*, **13**, 79 (2014).
4. Z. L. Wang and W. Wu, *Angrew. Chem. Int. Ed.*, **51**, 11700 (2012).
5. W. Zeng, L. Shu, Q. Li, F. Wang, and X.-M. Tao, *Adv.*

Mat., **36**, 5310 (2014).
6. C. R. Bowen, H. A. Kim, P. M. Weaver, and S. Dunn, *Energy Environ. Sci.*, **7**, 25 (2014).
7. R. T. Selvan, Y. J. Ahn, K. J. Kim, and H. Kim, *Fiber. Polym.*, **18**, 1898 (2017).
8. S.-H. Shin, Y.-H. Kim, M. H. Lee, J.-Y. Jung, J. H. Seol, and J. Nah, *ACS Nano*, **8**, 10844 (2014).
9. J. Yan and Y. G. Jeong, *ACS Appl. Mater. Interfaces*, **8**, 15700 (2016).
10. H. Y. Choi and Y. G. Jeong, *Compos. Pt. B-Eng.*, **168**, 58 (2019).
11. S. Gupta, D. Maurya, Y. Yan, and S. Priya in "Lead-Free Piezoelectrics" (S. Priya and S. Nahm Eds.), p.89, Springer, New York, 2012.
12. Z.-H. Lin, Y. Yang, J. M. Wu, Y. Liu, F. Zhang, and Z. L. Wang, *J. Phys. Chem. Lett.*, **3**, 3599 (2012).
13. S. K. Mahadeva, K. Walus, and B. Stoeber, *ACS Appl. Mater. Interfaces*, **6**, 7547 (2014).
14. S.-H. Shin, Y.-H. Kim, M. H. Lee, J.-Y. Jung, and J. Nah, *ACS Nano*, **8**, 2766 (2014).
15. A. Koka and H. A. Sodano, *Nat. Commun.*, **4**, 2682 (2013).
16. J. Yan and Y. G. Jeong, *Compos. Sci. Technol.*, **144**, 1 (2017).
17. X. Wang, X. Deng, H. Wen, and L. Li, *Appl. Phys. Lett.*, **89**, 162902 (2006).
18. T. Karaki, K. Yan, T. Miyamoto, and M. Adachi, *Japan. J. Appl. Phys.*, **46**, 4 (2007).
19. K. I. Park, S. Xu, Y. Liu, G. T. Hwang, S. J. Kang, Z. L. Wang, and K. J. Lee, *Nano Lett.*, **10**, 4939 (2010).
20. J. Briscoe and S. Dunn, *Nano Energy*, **14**, 15 (2015).
21. R. A. Whiter, Y. Calahorra, C. Ou, and S. Kar-Narayan, *Macromol. Mater. Eng.*, **301**, 1016 (2016).
22. J. Yan, M. Liu, Y. G. Jeong, W. Kang, L. Li, Y. Zhao, N. Deng, B. Cheng, and G. Yang, *Nano Energy*, **56**, 662 (2019).
23. R. Gregorio Jr., *J. Appl. Polym. Sci.*, **100**, 3272 (2006).
24. A. Salimi and A. A. Yousefi, *Polym. Test.*, **22**, 699 (2003).
25. A. J. Lovinger, *Science*, **220**, 1115 (1983).
26. W. Zhou, X. Jiang, P. Wang, and H. Wang, *Fiber. Polym.*, **14**, 100 (2013).
27. G. T. Davis, J. E. Mckinney, M. G. Broadhurst, and S. C. Roth, *J. Appl. Phys.*, **49**, 4998 (1978).
28. D. Farrar, K. Ren, D. Cheng, S. Kim, W. Moon, W. L. Wilson, J. E. West, and S. M. Yu, *Adv. Mat.*, **23**, 3954 (2011).
29. Y. R. Wang, J. M. Zheng, G. Y. Ren, P. H. Zhang, and C. Xu, *Smart Mater. Struct.*, **20**, 045009 (2011).
30. J. Fang, H. Niu, H. Wang, X. Wang, and T. Lin, *Energy Environ. Sci.*, **6**, 2196 (2013).
31. N. T. Tien, T. Q. Trung, Y. G. Seoul, D. I. Kim, and N.-E. Lee, *ACS Nano*, **5**, 7069 (2011).
32. D. Berlincourt and H. Jaffe, *Phys. Rev.*, **111**, 143 (1958).
33. H. Nagata, M. Yoshida, Y. Makiuchi, and T. Takenaka, *Japan. J. Appl. Phys.*, **42**, 7401 (2003).
34. H. Xu and L. Gao, *J. Am. Ceram. Soc.*, **86**, 203 (2003).
35. K. Uchino, E. Sadanaga, and T. Hirose, *J. Am. Ceram. Soc.*, **72**, 1555 (1989).
36. B. D. Begg, K. S. Finnie, and E. R. Vance, *J. Am. Chem. Soc.*, **79**, 2666 (1996).
37. Z. Lazarevic, N. Romcevic, M. Vijatovic, N. Paunovic, M. Rom·cevic, B. Stojanovic, and Z. Dohcevic-Mitrovic, *Acta Phys. Pol., A*, **115**, 808 (2009).
38. K. I. Park, M. Lee, Y. Liu, S. Moon, G. T. Hwang, G. Zhu, J. E. Kim, S. O. Kim, D. K. Kim, Z. L. Wang, and K. J. Lee, *Adv. Mater.*, **24**, 2999 (2012).
39. A. Pinczuk, W. Taylor, E. Burstein, and I. Lefkowitz, *Solid State Commun.*, **5**, 429 (1967).
40. M. DiDomenico Jr., S. H. Wemple, S. P. S. Porto, and R. P. Bauman, *Phys. Rev.*, **174**, 522 (1968).
41. M. H. Frey and D. A. Payne, *Phys. Rev. B*, **54**, 3158 (1996).
42. T. Boccaccio, A. Bottino, G. Capannelli, and P. Piaggio, *J. Membrane Sci.*, **210**, 315 (2002).
43. D. M. Esterly and B. J. Love, *J. Polym. Sci. Part B: Polym. Phys.*, **42**, 91 (2004).
44. H. T. Evans, Jr., *Acta Cryst*., **14**, 1019 (1961).
45. X. Chen, S. Xu, N. Yao, and Y. Shi, *Nano Lett.*, **10**, 2133 (2010).